MOLECULAR AND CELLULAR BIOLOGY, Oct. 2011, p. 4022–4035 Vol. 31, No. 19
0270-7306/11/$12.00 doi:10.1128/MCB.05289-11

Analysis of Human Syndromes with Disordered Chromatin Reveals the Impact of Heterochromatin on the Efficacy of ATM-Dependent G_2/M Checkpoint Arrest[▽]

Holly Brunton,[1] Aaron A. Goodarzi,[1] Angela T. Noon,[1] Amruta Shrikhande,[1] R. Scott Hansen,[2] Penny A. Jeggo,[1]* and Atsushi Shibata[1]*

Genome Damage and Stability Centre, University of Sussex, East Sussex BN1 9RQ, United Kingdom,[1] and Departments of Medicine and Genome Sciences, University of Washington, Seattle, Washington 98195[2]

Received 2 March 2011/Returned for modification 25 March 2011/Accepted 12 July 2011

Heterochromatin (HC) poses a barrier to γH2AX focus expansion and DNA double-strand break (DSB) repair, the latter being relieved by ATM-dependent KAP-1 phosphorylation. Using high-resolution imaging, we show here that the HC superstructure markedly restricts ATM signaling to cell cycle checkpoint proteins. The impact of HC is greater than anticipated from the percentage of HC-DNA and, in distinction to DSB repair, ATM only partly overcomes the constraints posed by HC. Importantly, we examine ATM signaling in human syndromes with disordered HC. After depletion of MeCP2 and DNMT3B, proteins defective in the Rett and immunodeficiency with centromere instability and facial anomalies (ICF) syndromes, respectively, we demonstrate enhanced γH2AX signal expansion at HC-chromocenters in mouse NIH 3T3 cells, which have visible HC-chromocenters. Previous studies have shown that the G_2/M checkpoint is inefficient requiring multiple DSBs to initiate arrest. MeCP2 and DNMT3B depletion leads to hypersensitive radiation-induced G_2/M checkpoint arrest despite normal DSB repair. Cell lines from Rett, ICF, and Hutchinson-Guildford progeria syndrome patients similarly showed hyperactivated ATM signaling and hypersensitive and prolonged G_2/M checkpoint arrest. Collectively, these findings reveal that heterochromatin contributes to the previously described inefficient G_2/M checkpoint arrest and demonstrate how the signaling response can be uncoupled from DSB repair.

The DNA damage response (DDR) to the presence of DNA double-strand breaks (DSBs) encompasses pathways of DSB repair and a signal transduction response that includes the activation of cell cycle checkpoint arrest and/or apoptosis. ATM-dependent signaling is the most significant signal transduction pathway activated by DSBs (19). An early step in the signaling pathway is the phosphorylation of H2AX, a step that can be effected by either ATM or DNA-PKcs. The damage response mediator proteins MDC1, RNF8, RNF168, and 53BP1 localize to the DSB, generating irradiation-induced foci (IRIF) (25, 26, 34). The precise function of IRIF remains unclear; cells lacking IRIF activate checkpoint arrest normally except at low doses where IRIF appear to function to amplify the signal. Most DSB repair occurs independently of ATM signaling but, critically, a subset of DSBs requires ATM and IRIF proteins for their repair (15, 28).

Over the past few years, a range of studies have demonstrated that chromatin structure exerts a significant impact on the DDR. For example, histone H1 restricts DDR signal amplification and reduced H1 levels confer hypersensitive G_2/M checkpoint arrest (23). That study provided initial evidence that the size of γH2AX foci determines the magnitude of the ATM signal and the sensitivity of G_2/M checkpoint arrest. In addition, studies have shown that both transcription and higher order chromatin structure can impact upon the expansion of γH2AX foci (8, 15, 17, 18). Of relevance to this work, it has been shown that γH2AX focus expansion is restricted by heterochromatin (HC) and that IRIF expand on the periphery rather than within HC regions (8, 15, 18). Further, despite the expansion of IRIF at the HC periphery, ATM-dependent signaling is required for the repair of HC-DSBs in contrast to DSBs located within euchromatic (EC) regions. Such repair requires ATM-dependent phosphorylation of the HC building factor, Kruppel-associated box (KRAB)-associated protein 1 (KAP-1) (24). Thus, the subset of DSBs that specifically require ATM for repair represent HC-DSBs. Interestingly, recent findings have also shown the HC restricts DSB repair by homologous recombination in *Drosophila*, although there are differences to the situation in mammalian cells (7). First, HC-DSB repair in *Drosophila* is predominantly ATR dependent. Further, the phosphorylation site on KAP-1 does not appear to be conserved in *Drosophila*. Thus, while HC represents a barrier to repair in both organisms, the way of overcoming this may differ to some extent. In mammalian cells, although γH2AX foci do not expand within the center of densely staining DAPI chromocenters, they appear to expand normally at their periphery albeit with restricted encroachment into the HC superstructure. Indeed, no difference in the size of γH2AX foci at EC and HC DSBs is apparent or has been reported. Thus, although ATM-dependent KAP-1 phosphorylation is required to enable repair of HC-DSBs, it is unclear whether the HC superstructure actually impacts upon ATM signaling to the checkpoint machinery.

G_2/M checkpoint arrest, a crucial endpoint of ATM signaling, coordinates DSB formation and repair with cell cycle pro-

* Corresponding author. Mailing address: Genome Damage and Stability Centre, University of Sussex, East Sussex BN1 9RQ, United Kingdom. Phone: 44 1273 678482. Fax: 44 1273 678121. E-mail for Atsushi Shibata: as303@sussex.ac.uk. E-mail for Penny A. Jeggo: p.a.jeggo@sussex.ac.uk.

▽ Published ahead of print on 26 July 2011.

gression. The G_2/M checkpoint has a defined sensitivity and, as a consequence, is not activated by low radiation doses (10, 13). The same concept also results in the release of cells from checkpoint arrest prior to completion of DSB repair. The magnitude of ATM signaling and the impact on the initiation and maintenance of checkpoint arrest is thus responsive to the progress of DSB repair; hence, defects that impair DSB repair result in prolonged ATM signaling and checkpoint arrest. The recent analysis of factors that influence chromatin modifications such as HDAC1/2 and CHD4 have shown that they can have an impact on both DSB repair and signal expansion, with enhanced signaling likely being a consequence of impaired DSB repair (22, 27). In the first part of the present study, we examine whether HC superstructure modulates the magnitude of ATM signaling to cell cycle checkpoint arrest. In contrast to the situation above where DSB repair is impaired, we examine situations where the rate of DSB repair is unperturbed. We observed that depletion of factors required for the building of the HC superstructure confers enhanced ATM signal expansion at HC-DSBs compared to that arising at EC-DSBs. Unexpectedly, this resulted in hypersensitive and prolonged G_2/M checkpoint arrest. These findings provide the first evidence that the HC superstructure exerts a significant impact upon checkpoint arrest independently of any impact on DSB repair, uncoupling checkpoint signaling from repair.

How HC superstructure influences the DDR is important to evaluate, not least because the HC content can differ between tissues and cell types. Further, human syndromes with disordered HC structure have been reported. These syndromes include (i) Rett syndrome, which harbors mutations in MeCP2, a methyl CpG-binding protein, (ii) immunodeficiency with centromere instability and facial anomalies (ICF) syndrome, which is mutated in the DNA methyltransferase, DNMT3B, and (iii) Hutchinson-Gilford progeria syndrome (HGPS), which has mutations in lamin A and displays progressive HC loss (3, 5, 9, 31). The HC superstructure involves a self-reinforcing web of histone and DNA modifications constructed with additional factors or complexes that have chromatin remodeling activity. KAP-1 functions as a scaffold protein and targets the KRAB-ZFP superfamily, thereby coordinating histone methylation and the deposition of HP1 (4). Methylation at CpG islands contributes to gene silencing due, in part, to the recruitment of methyl-CpG-binding protein 2 (MeCP2), which interacts with HDAC1/2 and additional corepressor proteins (1). MeCP2 also directly interacts with HP1 (2).

In the second part of our study, we examine whether disordered HC in patient cells impacts upon ATM signaling to cell cycle checkpoint arrest. Importantly, in these syndromes, the rate of DSB repair is identical to that observed in control, although the requirement for ATM is partly overcome. Strikingly, despite a normal rate of DSB repair in these syndrome cells, we observe hypersensitive and prolonged G_2/M checkpoint arrest. Our findings show that HC exerts a substantial impact on the magnitude of ATM signaling and contributes to the previously described inefficient G_2/M checkpoint response.

MATERIALS AND METHODS

Cell culture, drug treatment, and irradiation. 48BR (wild type) and GM16548, GM11271, and GM11272 (Rett/MeCP2) primary human fibroblasts, as well as 1BR hTERT, PT3 (ICF/DNMT3B), and P2 (XLF) hTERT cells, were cultured in Dulbecco modified Eagle medium with 15% fetal calf serum (FCS). GM02188 (wild type), GM16548 (Rett/MeCP2), GM08714 (ICF/DNMT3B), and AG10801 (HGPS/Lamin A) are lymphoblastoid cell lines (LBLs) and were cultured in RPMI with 10% FCS. NIH 3T3, murine embryonic fibroblast (MEF), and A549 cells were cultured in minimal essential medium with 10% FCS. All culture medium are supplemented with L-glutamine, penicillin, and streptomycin. ATM inhibitor at 10 μM (Calbiochem) and the Chk1/Chk2 inhibitor, SB218078 (Tocris Bioscience), at 2.5 μM were added 30 min before irradiation (IR). Cells were irradiated in medium by using either a ^{137}Cs gamma source (dose rate, 7.5 Gy/min) or 250-kV X rays delivered at 12 mA (dose rate, 0.5 Gy/min).

siRNA knockdown and MeCP2 expression. Small interfering RNA (siRNA) transfection of 48BR, 1BR hTERT, A549, and NIH 3T3 cells was undertaken using Metafectene Pro (Biotex, Germany) or Hiperfect (Qiagen, Hilden, Germany) according to the manufacturer's instructions. Scramble control, mouse MeCP2, and mouse DNMT3B were from Dharmacon SMART pool siRNA. Two distinct human MeCP2 and DNMT3B siRNA oligonucleotides were obtained from Invitrogen. The sequence of human and mouse KAP-1 siRNA is as described previously (15). siRNA knockdown was carried out in suspended cells after trypsinization. After 24 h, cells were treated with trypsin and retransfected with siRNA. Cells were incubated for 48 h after the second transfection prior to analysis. The MeCP2-expressing vector (pEGFP-MeCP2) was kindly provided by Adrian Bird. Wild-type (WT) EGFP-MeCP2 was expressed in Rett LBLs using GeneJuice (Novagen/Merck, Germany) according to the manufacturer's instructions. To express WT MeCP2 in MeCP2 siRNA cells, three mutations within the siRNA target sequence were introduced in MeCP2 cDNA by using a QuikChange site-directed mutagenesis kit (Invitrogen). pEGFP-MeCP2 plasmid was transfected into cells for 6 h, 24 h after siRNA knockdown of 1BR hTERT cells. After incubation at 37°C for 16 to 24 h, the cells were irradiated and analyzed.

Immunofluorescence and immunoblotting. Immunofluorescence and immunoblotting were performed with antibodies against γH2AX (Upstate Technology, United Kingdom), 53BP1 (Bethyl Laboratories, Montgomery, AL), p-histone H3 (p-H3) Ser10 (Upstate Biotechnology, Buckingham, United Kingdom), Chk2 pThr68 (Cell Signaling Technology, Beverly, MA), Chk2 (Abcam, Cambridge, United Kingdom or Cell Signaling Technology), KAP-1 (Abcam), Ku70 (Santa Cruz Biotechnology, Santa Cruz, CA), ATM pSer1981 (Epitomics, Burlingame, CA), ATM (Cell Signaling Technology), ATR (Santa Cruz), Chk1 (Cell Signaling Technology), p53 (Santa Cruz), Ku80 (polyclonal rabbit antibody), actin (Abcam), and CENP-F (Abcam). For immunofluorescence, coverslips were visualized by using a Zeiss Axioplan microscope and simple PCI software. An Applied Precision DeltaVision RT Olympus IX70 deconvolution microscope and softWoRx Suite software was used for high-resolution and three-dimensional imaging of deconvolved z-stacks.

Analysis of signal intensity by ImageJ and softWoRx Suite software. The signal intensity of fluorescein isothiocyanate and DAPI (4′,6′-diamidino-2-phenylindole) per γH2AX focus was quantified with ImageJ (see Fig. 2C and 4C). In the pChk2 and pATM signal intensity analyses (see Fig. 3C and 6D), the untreated nuclear intensity was subtracted from the IR-induced nuclear signal intensity. The images were taken by the Zeiss Axioplan microscope with an identical exposure time. The size of γH2AX foci at the chromocenter in Fig. 2E and 4E was quantified with ImageJ after deconvolution with softWoRx Suite software. Quantitative measurements of γH2AX and DAPI overlap were obtained and visualized as a red signal using softWoRx Suite software. The size of overlapping regions per cell was quantified by ImageJ. The number of chromocenters was analyzed and showed similar between cell lines (data not shown). The size of overlap per chromocenter was normalized following these analyses. The volume of the interior signal was visualized and measured by Huygens Professional, Scientific Volume Imaging. Similar to the analysis of overlap, the volume per chromocenter was normalized to the number of chromocenters (see Fig. 2F and 4F).

γH2AX foci and G_2/M checkpoint analysis. DSB repair was monitored by disappearance of γH2AX foci (21). G_1- and G_2-phase cells were identified by using the cell cycle marker, anti-CENPF in human cells and anti-p-H3 Ser10 in mouse cells, respectively (6). S-phase cells show a mild CENPF signal, whereas G_2-phase cells show substantially greater signal. M-phase cells are identified by their morphological changes, i.e., condensed chromatin by DAPI. For DSB repair in cycling cells and maintenance of G_2/M checkpoint analysis, 4 μM aphidicolin (APH) was added immediately after IR to block the entry of irradiated S-phase cells into G_2 during analysis. Replication in the presence of APH induces extensive γH2AX signaling, which helps the identification of S-phase cells during γH2AX focus analysis. APH does not impact upon DSB repair and signaling in the G_1 and G_2 phases (6, 21, 30). For initiation of G_2/M checkpoint analysis, the cells were fixed 1 or 2 h after IR and stained for p-H3 Ser10 and

DAPI. p-H3 Ser10-positive and condensed chromatin cells were counted as the mitotic index. More than 400 cells were scored per condition.

Trimethylated K9 of histone H3 immunoprecipitation (IP). After IR, 5×10^6 LBLs were washed with phosphate-buffered saline (PBS) and then with low-salt buffer (LSB) (10 mM HEPES [pH 7.4], 25 mM KCl, 10 mM NaCl, 1 mM $MgCl_2$, 0.1 mM EDTA). Pelleted cells were resuspended in LSB plus phosphatase and a protease inhibitor cocktail (Sigma-Aldrich, United Kingdom) and snap-frozen in liquid nitrogen. The cells were quick thawed and immediately centrifuged for 10 min at 10,000 rpm. The pellet was resuspended and treated with 100 U of MNase/ml in nuclease buffer (10 mM HEPES [pH 7.9], 10 mM KCl, 1.0 mM $CaCl_2$, 1.5 mM $MgCl_2$, 0.34 M sucrose, 10% glycerol, 1 mM dithiothreitol, 0.1% [vol/vol] Triton X-100). After incubation at 37°C for 45 min, an equal volume of solubilization buffer (nuclease buffer plus 2% [vol/vol] NP-40, 2% [vol/vol] Triton X-100, 600 mM NaCl) was added. Samples were then briefly sonicated and centrifuged at 10,000 rpm for 10 min. The resulting supernatant containing solubilized nucleosomes (50 μg) was incubated with 2 μg of chromatin IP-grade α-TriMe K9 histone H3 monoclonal antibody (Abcam) overnight at 4°C. Immunocomplexes were pulled down by adding protein G- and A-Sepharose (1:1) for 30 min at 4°C. The samples were boiled for 3 min before electrophoresis in SDS-PAGE.

PFGE. Cells were exposed to 20 Gy of IR and treated with trypsin at the times indicated, washed twice with PBS, and then embedded in 0.75% low-melting-agarose gel plugs (SeaPlaque Agarose; Cambrex Bioproducts) at a concentration of 0.75×10^5 cells/plug. Plugs were placed in buffer containing 20 μg of proteinase K/ml, 0.5 M EDTA, and 1% Sarkosyl (pH 9.0), followed by incubation at 50°C for 24 h in the dark. Plugs were washed with 50 mM EDTA at room temperature for 1 h and stored at 4°C. Pulsed-field gel electrophoresis (PFGE) was carried out using a CHEF Mapper (Bio-Rad), with a cooling module (model 1000 Mini Chiller; Bio-Rad) in 1% agarose gels (pulsed-field certified agarose; Bio-Rad) in 0.5× Tris-borate-EDTA. The forward and reverse voltage gradients were 5.4 and 3.6 V/cm, respectively, for 5 to 60 s for a total of 20 h at 14°C. After PFGE, the gels were stained with ethidium bromide and photographed under UV transillumination. The signal intensity of the smear was quantified by ImageJ at each time point and normalized to the intensity at 15 min after IR.

RESULTS

KAP-1 depletion enhances the expansion of HC-associated γH2AX foci. Previous studies have shown that γH2AX foci do not expand into HC regions and that HC can restrict DSB repair (8, 15, 18). siRNA-mediated depletion of KAP-1, which is a HC building factor, does not affect the rate of DSB repair in control cells but bypasses the requirement for ATM (15). Here, we examined whether depletion of KAP-1 and other HC factors has an impact upon γH2AX signal expansion at HC-DSBs. First, we compared the kinetics of IR-induced γH2AX focus formation at the HC and EC regions by using NIH 3T3 cells, which have readily visualized dense DAPI staining chromocenters that correspond to pericentromeric and centromeric HC (15, 16). We defined γH2AX foci that overlap/juxtapose or do not overlap with chromocenters as HC and EC associated foci, respectively (Fig. 1A). To directly compare the speed of focus formation at EC versus HC-DSBs, we enumerated γH2AX foci for up to 20 min post-IR when the focus numbers become maximal (Fig. 1B to D). Significantly, we show that the kinetics of γH2AX formation is dose independent and occurs more rapidly at the EC than at the HC-DSBs (Fig. 1E).

We next examined whether the loss of KAP-1 temporally affects the appearance of γH2AX focus formation after IR. Although KAP-1 siRNA does not significantly change the size or structure of chromocenters (data not shown), it specifically enhances the rate of focus formation at the HC-DSBs (Fig. 2A and B). To assess the size of γH2AX foci, we monitored the signal intensity at foci of different DAPI signal intensities following control or KAP-1 siRNA at 30 min post-IR, a time when maximal focus numbers have been reached. We arbitrarily defined regions of high and low DAPI signal as representing HC or EC regions. Although an inexact definition, it allows the impact of chromatin compaction to be assessed. Initially, we carried out a two-dimensional analysis of the size of individual foci. In control cells, the focus size at 30 min post-IR was independent of DAPI signal intensity. Thus, despite their slower rate of formation, foci at the HC-DSBs reach a similar size to those at the EC-DSBs by 30 min. KAP-1 siRNA significantly increased the γH2AX signal intensity at the DAPI regions of higher density relative to those of lower density, where no significant impact of KAP-1 siRNA was observed (Fig. 2C). Surprisingly, the signal intensity in the regions of high DAPI signal following KAP-1 depletion was greater than in the regions of lower DAPI signal and greater than observed in control cells (see the Discussion for possible explanations). This suggests that ATM signaling either does not fully relieve the barrier posed by HC to focus expansion or does so inefficiently. To engineer the loss of ATM signaling specifically at the HC-DSBs, we examined the impact of 53BP1 knockdown, since we have previously shown that 53BP1 increases the retention of ATM at the DSBs specifically promoting pKAP-1 focus formation at KAP-1-rich HC-DSBs; it does not impair pan-nuclear pKAP-1 since 53BP1 only slightly reduces overall ATM signaling (24). Significantly, 53BP1 siRNA resulted in a greater decrease in the sizes of γH2AX foci at the HC compared to the EC regions (Fig. 2C). This suggests that ATM-dependent pKAP-1 accumulation at the HC-DSBs enhances γH2AX focus size but does not fully overcome the barrier posed by the HC superstructure. In contrast, ATM inhibitor (ATMi) treatment reduced γH2AX focus size irrespective of the DAPI density (Fig. 2C).

Thus, the global HC relaxation following KAP-1 knockdown provides a greater level of focus expansion than that observed in control cells despite ATM activation. This is likely because in control cells pKAP-1 formation around a DSB only causes HC relaxation in the DSB vicinity, whereas KAP-1 knockdown causes more extensive HC relaxation.

To assess further the impact of HC on γH2AX focus expansion, we quantified the magnitude of the γH2AX-chromocenter overlap using high-resolution deconvolved z-stacked images in KAP-1-depleted cells (this also represents a two-dimensional analysis) (Fig. 2D) (we did not perform this analysis in 53BP1 siRNA- or ATMi-treated cells because of the tiny size of the foci at HC regions). We observed a >3-fold increase in the magnitude of the γH2AX focus-chromocenter overlap following the addition of KAP-1 siRNA (Fig. 2E). To examine whether this represents expansion of the foci on the surface of chromocenters or into the HC interior, we measured the volume of γH2AX signal within the HC interior using three-dimensional modeling software (Fig. 2F). Strikingly, we observed substantially greater γH2AX-DAPI overlap within the interior of chromocenters following the addition of KAP-1 siRNA. Collectively, these findings show that HC confers a substantial barrier to both the speed of formation and expansion of γH2AX foci and ATM signaling partly but does not fully overcome this barrier. Despite this, γH2AX foci formed at the HC and EC regions are of similar sizes largely due to the expansion of HC foci into the neighboring EC region.

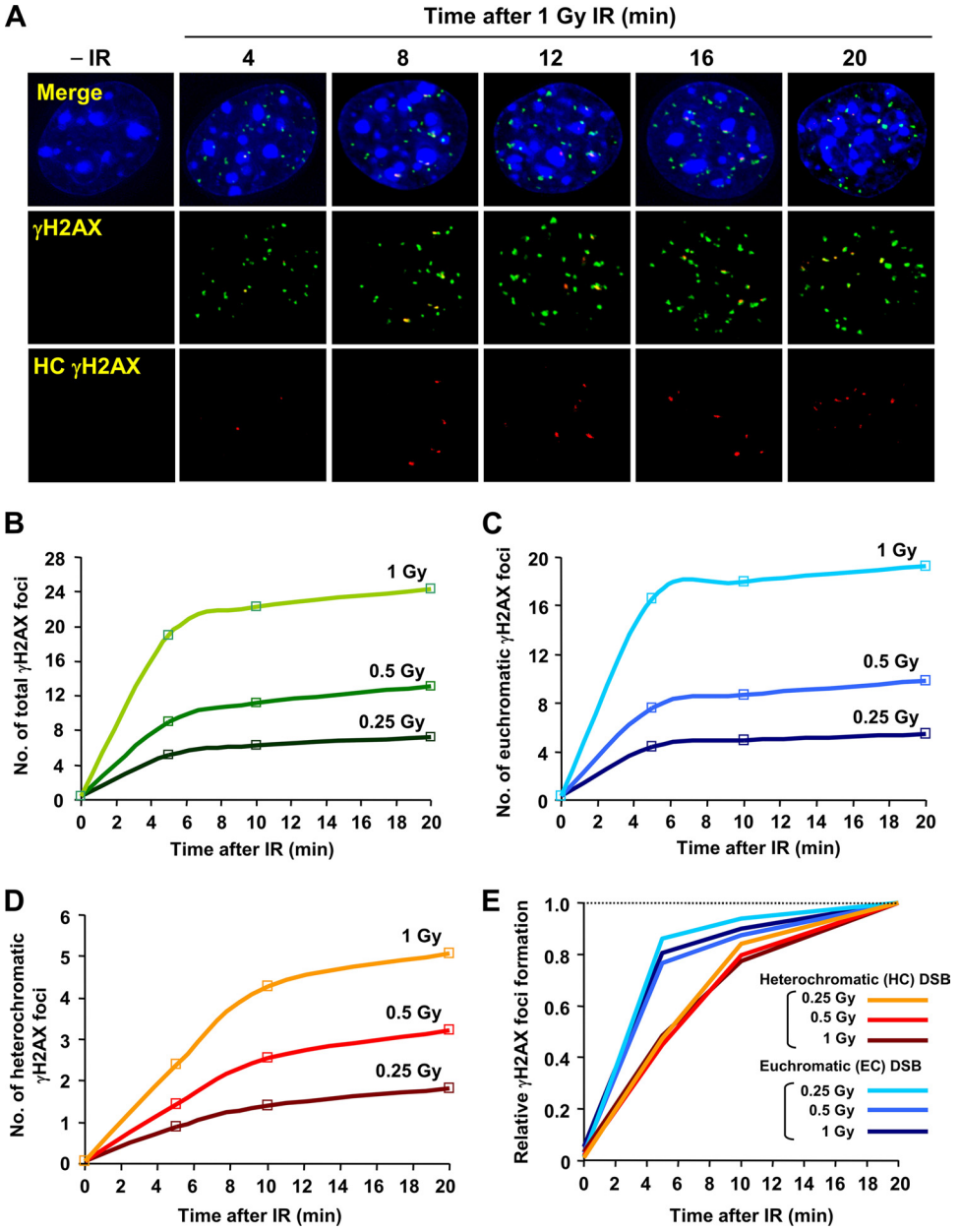

FIG. 1. Rate of γH2AX focus formation at HC and EC regions. (A) Typical images of γH2AX focus formation after IR in NIH 3T3 cells. HC γH2AX (red) represents regions of γH2AX and dense DAPI chromocenter overlap, as determined by softWoRx Suite software. (B to D) The rates of total (B), EC (C), and HC (D), γH2AX focus formation were enumerated after 0.25, 0.5, and 1 Gy of IR. (E) γH2AX focus formation is normalized to the 20 min post-IR signal. Similar results have been obtained in more than three independent experiments (see Fig. 2 and 4).

Depletion of KAP-1 enhances ATM signaling and G_2/M checkpoint sensitivity. We next examined whether the enhanced γH2AX focus expansion at chromocenters that we observed following the addition of KAP-1 siRNA correlates with enhanced checkpoint signaling and arrest. To monitor checkpoint signaling, we examined IR-induced Chk2 phosphorylation (pChk2) by Western blotting and observed increased pChk2 after KAP-1 depletion (Fig. 3A). The ATM dependency of Chk2 activation was confirmed by using ATMi (Fig. 3B). As shown by immunofluorescence (IF), KAP-1-depleted cells showed a 2- to 3-fold increase in pChk2 levels compared to the control after IR (Fig. 3C). We also examined the sensitivity of G_2/M checkpoint arrest following the addition of KAP-1 siRNA, exploiting our previous findings that checkpoint arrest in control cells is not initiated after low IR doses (10). Cells were transfected with control or KAP-1 siRNA in WT or $ATM^{-/-}$ MEFs, and G_2/M checkpoint arrest was monitored by scoring phospho-histone H3 Ser10-positive cells 1 h after IR. G_2/M arrest was abolished in $ATM^{-/-}$ MEFs irrespective of the KAP-1 status (Fig. 3D), confirming that G_2/M checkpoint arrest is ATM dependent. Importantly, KAP-1-depleted cells showed hypersensitive checkpoint arrest at

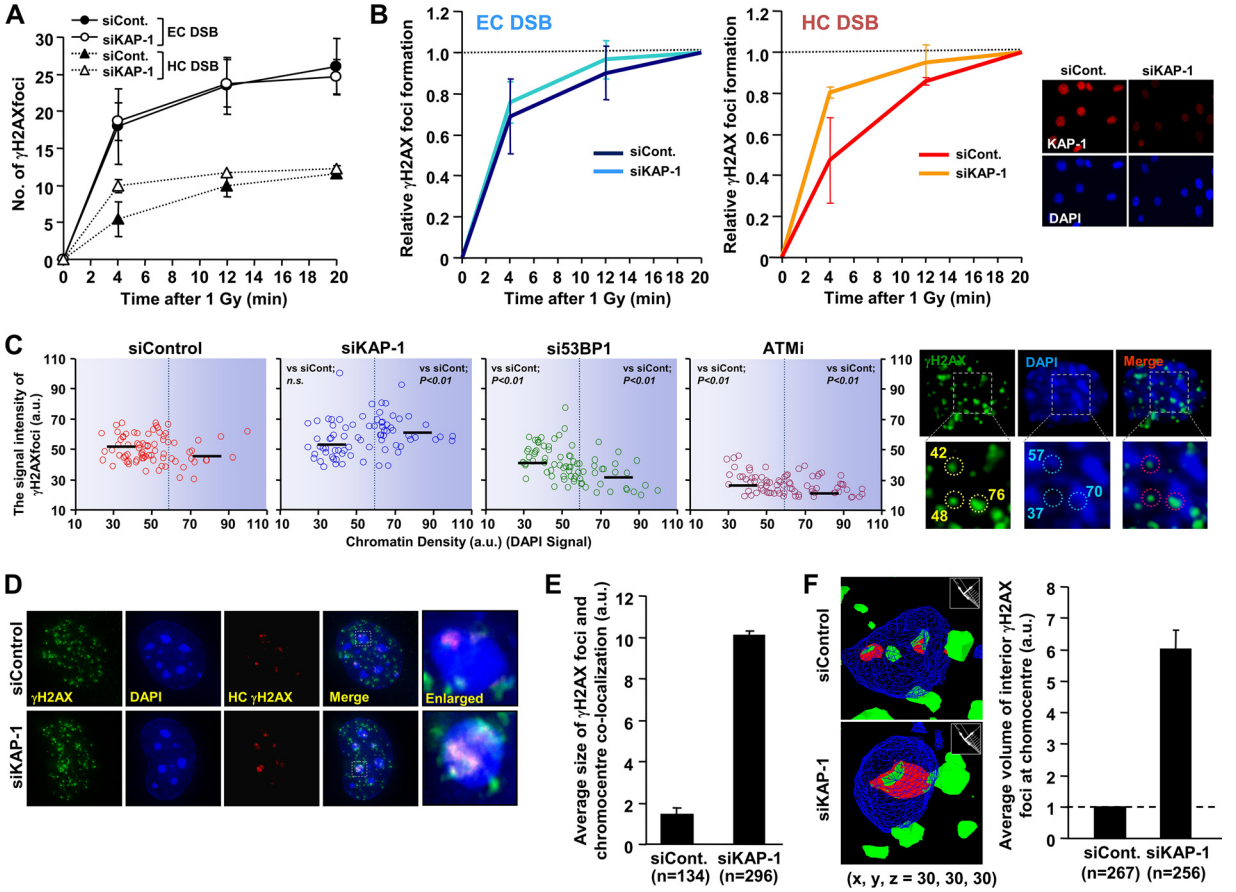

FIG. 2. Depletion of KAP-1 enhances the speed and expansion of γH2AX signal at HC regions. (A) KAP-1 siRNA increases the speed of HC γH2AX focus formation. KAP-1 siRNA-treated NIH 3T3 cells were irradiated with 1 Gy. The numbers of γH2AX foci overlapping/juxtaposing and nonoverlapping with chromocenters were enumerated as HC and EC foci. (B) The rate of γH2AX focus formation shown in panel A was normalized to the number of foci at 20 min. The KAP-1 knockdown efficiency is shown in right panel. (C) Greater γH2AX signal intensity at higher-density DAPI regions in KAP-1 siRNA-treated cells after IR. KAP-1 siRNA treated NIH 3T3 cells were irradiated with 3 Gy of IR and fixed 30 min later. The signal intensity of γH2AX and DAPI per focus was quantified by using ImageJ. Typical images and values are shown in the right panel. Black bars represent the median. The statistical significance was determined using Student two-tailed *t* test. (D and E) Increased γH2AX signal expansion at HC regions following KAP-1 siRNA. High-resolution deconvolved z-stacked images in KAP-1-depleted NIH 3T3 cells are shown in panel D. γH2AX signal overlap of with dense DAPI (blue plus green) was visualized as red signal determined by softWoRx Suite software computer analysis. The magnitude of overlap of γH2AX per chromocenter was quantitatively measured by using ImageJ. (F) Depletion of KAP-1 enhances signal expansion into the HC interior. The γH2AX signal expansion into the HC interior is shown by three-dimensional modeling in NIH 3T3 cells. The volume of the interior signal per chromocenter was measured by Huygens Professional, Scientific Volume Imaging. The quantification is shown in the right panel. In panels A to F, G_1 cells with negative staining for p-H3 Ser10 were analyzed. S-phase cells, which show extensive γH2AX signal, were excluded. Error bars represent the standard deviations (SD) from two independent experiments (A, B, E, and F). *n*, number of chromocenters analyzed (E and F).

lower doses compared to control cells. We consolidated this result in human A549 cells using a different KAP-1 siRNA oligonucleotide with or without ATMi addition (Fig. 3E). Similar to the results in MEFs, KAP-1 siRNA-treated cells were fully arrested after low doses, whereas control cells do not fully activate checkpoint arrest (Fig. 3E). We also observed similar hypersensitive checkpoint arrest following combined HDAC1/2 siRNA (Fig. 3E). Collectively, these results demonstrate that the increased γH2AX signal expansion following KAP-1 siRNA correlates with more sensitive G_2/M checkpoint arrest. In contrast, KAP-1 siRNA does not influence the kinetics or extent of DSB repair in control cells but merely overcomes the need for ATM (15). Since KAP-1 siRNA could exert multiple impacts leading to abnormal checkpoint arrest, we next examined whether a similar effect was observed following the loss of other factors required for the HC superstructure.

Depletion of MeCP2 and DNMT3B causes faster γH2AX focus formation and increased signal expansion in NIH 3T3 cells. DNA methylation at CpG islands (CGIs) is an important epigenetic modification that regulates gene silencing and chromatin compaction. DNA methylation at CGIs recruits the methyl-binding domain proteins, which recruit additional chromatin remodelers to silence chromatin (35). Here, we focused on changes in methylation-dependent chromatin compaction caused by the loss of methyl CpG-binding protein 2 (MeCP2) or DNA methyltransferase 3B (DNMT3B), since they represent components mutated in human syndromes (see below). Prior to examining patient cell lines, we examined the

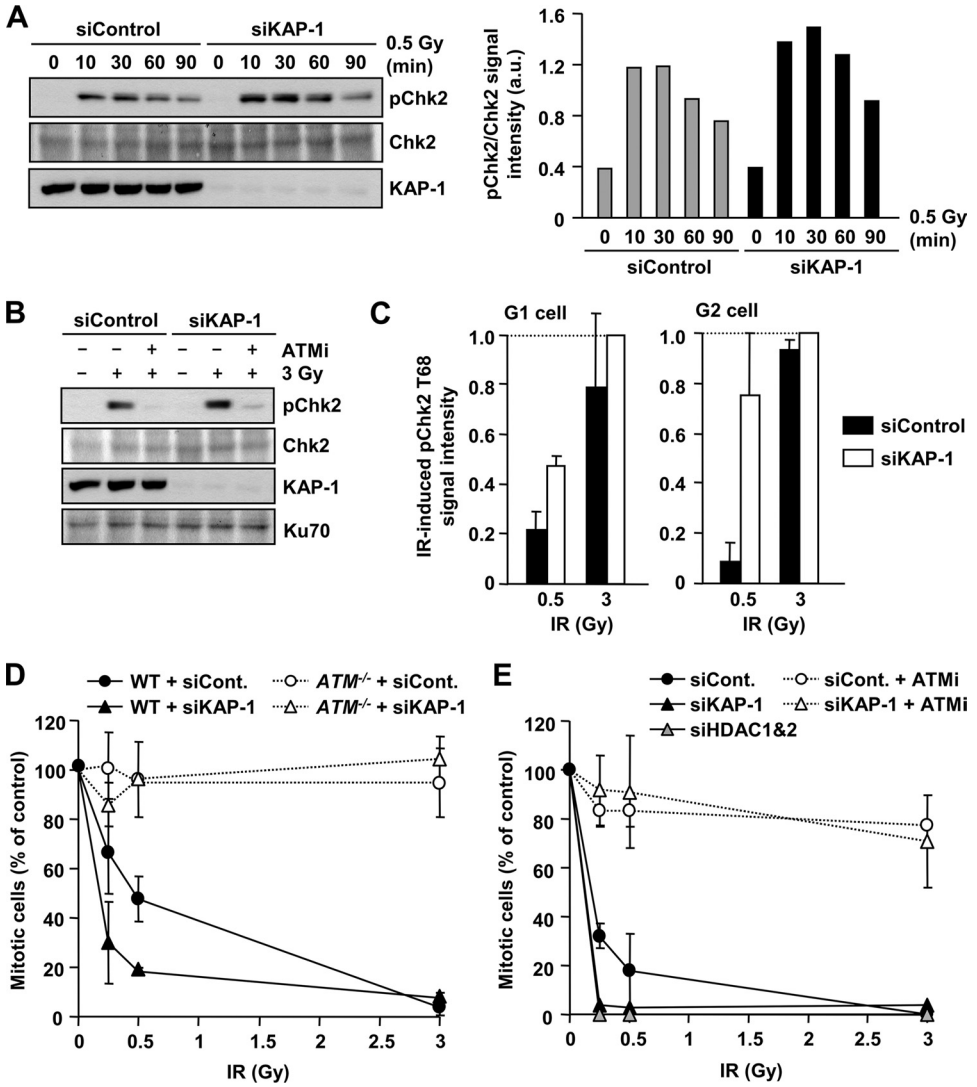

FIG. 3. KAP-1 depletion enhances ATM signaling and G_2/M checkpoint sensitivity. (A) Increased pChk2 is observed following KAP-1 depletion after IR. 1BR (WT) hTERT cells with or without KAP-1 siRNA were exposed to 0.5 Gy IR and harvested at the indicated time points. Quantification of the pChk2 bands normalized by total Chk2 is shown in right panel. Similar results were observed in two additional experiments. (B) IR-induced pChk2 is ATM dependent irrespective of KAP-1 status. 1BR (WT) hTERT cells with or without KAP-1 siRNA were exposed to 3 Gy of IR with or without 10 μM ATM inhibitor and harvested 2 h post-IR. (C) Enhanced pChk2 signal is observed in KAP-1 depleted cells by IF. 1BR (WT) hTERT cells with or without KAP-1 siRNA were fixed and stained with pChk2, CENPF, and DAPI 30 min after IR. The signal intensity was analyzed by using ImageJ. G_2-phase cells were identified by CENP-F. Anti-pChk2 antibody specificity was confirmed as described previously (30). The results represent the mean ± the SD from two experiments. (D) KAP-1 siRNA knockdown causes hypersensitive G_2/M checkpoint arrest. WT and $ATM^{-/-}$ MEFs were subjected to KAP-1 siRNA. After IR, cells were fixed 1 h later and stained with anti-p-H3 Ser10 and DAPI. The numbers of p-H3 $Ser10^+$ cells were scored and normalized to the nonirradiated control. (E) KAP-1 and HDAC1/2 depletion increase the sensitivity of G_2/M checkpoint arrest. A549 cells were subjected to KAP-1 siRNA with or without ATMi or HDAC1/2 double siRNA. The percent mitotic cells 2 h after IR were scored. The results represent the means and the SD from three experiments (D and E).

impact of siRNA-mediated knockdown since the mutations in patients are likely hypomorphic and may be less impacting.

First, we found that neither depletion of MeCP2 nor DNMT3B by siRNA impacted the rate of DSB repair in mouse and human cells (data not shown [but see Fig. 5]). Next, we used siRNA-treated NIH 3T3 cells to examine whether methylation-dependent chromatin compaction affects IR-induced γH2AX focus formation at the HC regions. Similar to the results following KAP-1 siRNA, depletion of either MeCP2 or DNMT3B resulted in more rapid HC γH2AX focus formation after IR (Fig. 4A and B). Moreover, MeCP2 and DNMT3B siRNA caused a statistically significant increase in γH2AX signal intensity, with the effect being greater on the foci associated with higher-density DAPI regions (Fig. 4C). In some distinction to the findings following KAP-1 loss, the impact, particularly following the addition of MeCP2 siRNA, was also upon regions of intermediate DAPI density, possibly due to the role of methylation as a transcriptional repressor at the CGIs at both constitutive and facultative HC. In contrast, KAP-1 is primarily enriched within constitutive HC. We also analyzed

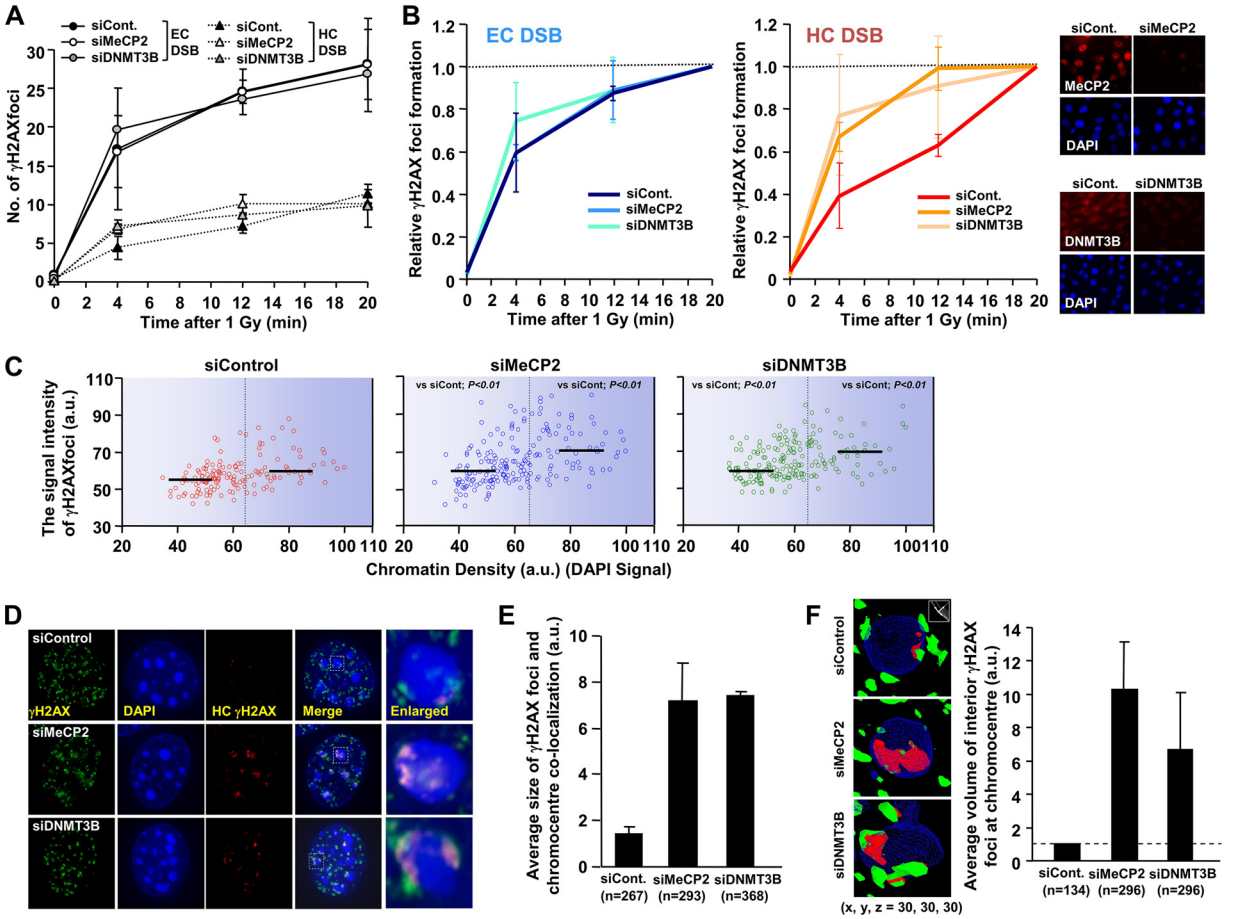

FIG. 4. Depletion of MeCP2 and DNMT3B allows increased γH2AX signal expansion. (A) Depletion of MeCP2 and DNMT3B increases the speed of HC γH2AX focus formation. MeCP2 and DNMT3B siRNA-treated NIH 3T3 cells were irradiated with 1 Gy and fixed at the indicated times. γH2AX focus formation was analyzed as described for Fig. 2. (B) The rate of γH2AX focus formation shown in panel A was normalized to the focus numbers counted at 20 min. The knockdown efficiencies are shown in the right panel. (C) MeCP2 and DNMT3B depletion with siRNA enhances γH2AX signal intensity at the HC regions. NIH 3T3 cells were subjected to siRNA irradiated with 3 Gy, fixed 30 min later, and stained with anti-γH2AX and DAPI. The signal intensity of γH2AX and DAPI per focus was quantified by using ImageJ. The black bars represent the median. The statistical significance was determined by using a Student two-tailed *t* test. (D and E) Increased γH2AX signal expansion at the HC regions following MeCP2 and DNMT3B siRNA. The regions of γH2AX-chromocenter overlap were analyzed as described for Fig. 2. (F) Depletion of MeCP2 and DNMT3B enhances the γH2AX signal expansion into the HC interior in NIH 3T3 cells. The γH2AX signal expansion within DAPI chromocenters in MeCP2 and DNMT3B siRNA-treated cells was measured as described for Fig. 2. G_1 cells negative for p-H3 Ser10 were analyzed (A to F). The results represent the means and the SD from two experiments (A, B, E, and F). *n*, number of chromocenters analyzed (E and F).

the extent of γH2AX and DAPI overlap in high-resolution deconvolved z-stacked images (Fig. 4D). Although we observed minor changes in the number of chromocenters in MeCP2- and DNMT3B-depleted cells (data not shown), computational analysis of γH2AX and DAPI overlap per chromocenter revealed an ~3-fold increase in γH2AX focus expansion following MeCP2 or DNMT3B siRNA (Fig. 4E). In addition, three-dimensional image analyses revealed a greater volume of overlap between γH2AX and HC within the interior of chromocenters (Fig. 4F). Collectively, these data demonstrate that MeCP2- and DNMT3B-dependent chromatin organization also creates a barrier to IR-induced γH2AX focus expansion at the HC regions since the depletion of MeCP2 or DNM3T enhances focus expansion into the HC core.

Loss of MeCP2/DNMT3B alleviates the ATM dependency of DSB repair. We observed, by using γH2AX focus analysis and PFGE (Fig. 5A and B), that despite the impact on ATM signaling (Fig. 4), IR-induced DSBs are repaired with normal kinetics following the addition of MeCP2 or DNMT3B siRNA. We also observed normal DSB repair kinetics after IR in three primary G_0/G_1 fibroblasts derived from Rett syndrome patients (Fig. 5C). We previously reported that loss of HC building factors (e.g., KAP-1, HP1, or HDAC1/2) overcomes the requirement for ATM for DSB repair (15). We, therefore, examined whether MeCP2 deficiency in Rett cells alleviates the DSB repair defect conferred by the addition of ATMi. Surprisingly, the loss of MeCP2 activity in Rett cell lines does not affect DSB repair kinetics in the presence of ATMi (Fig. 5C). In contrast, MeCP2 siRNA, while not affecting DSB repair in the absence of ATMi, almost entirely alleviated the DSB repair defect conferred by ATMi addition in WT and Rett cell lines in the G_1 and G_2 phases (Fig. 5D and E). These

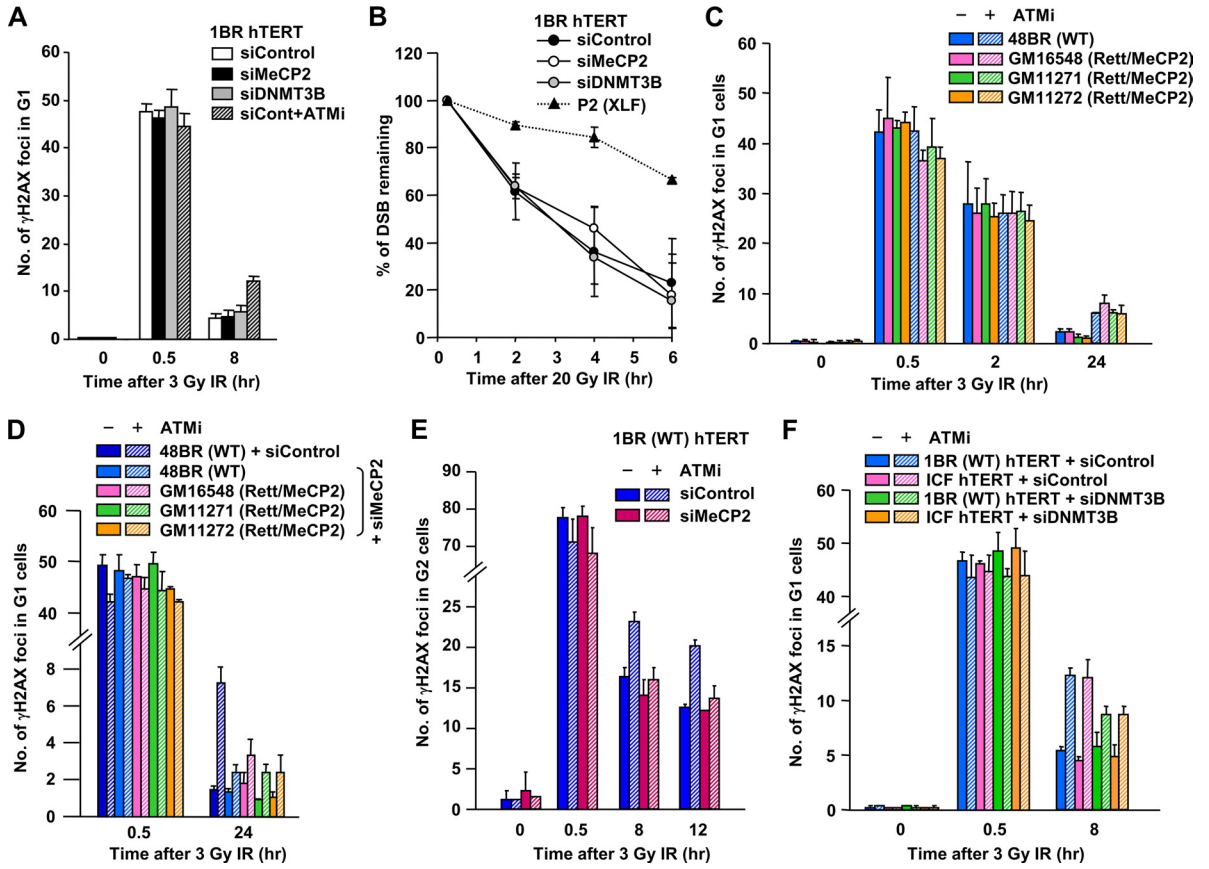

FIG. 5. Rett and ICF syndrome cell lines show a normal rate of DSB repair; MeCP2 and DNMT3B depletion alleviates the DSB repair defect conferred by ATMi treatment. (A) Depletion of MeCP2 and DNMT3B does not influence DSB repair kinetics in 1BR (WT) hTERT cells. To assess the impact of ATM on DSB repair, ATMi was added 30 min prior to IR. A similar result was observed in MeCP2- and DNMT3-depleted NIH 3T3 cells (data not shown). (B) DSB repair was also analyzed by neutral PFGE after 20 Gy of IR. P2 (XLF) hTERT cells show a substantial DSB repair defect, whereas MeCP2-, DNMT3B siRNA-treated 1BR (WT) hTERT cells show normal DSB repair after IR. (C) Rett primary fibroblasts show normal DSB repair in G_1 phase, and the hypomorphic MeCP2 mutations in Rett cells do not overcome the DSB repair defect in ATMi-treated cells. (D) Depletion of MeCP2 with siRNA alleviates the DSB repair defect in G_1 phase conferred by ATMi treatment in Rett primary fibroblast cells. MeCP2 siRNA was undertaken in control and Rett fibroblasts. (E) Depletion of MeCP2 does not affect DSB repair in G_2-phase cells but rescues the repair defect conferred by ATMi addition. 1BR (WT) hTERT cells were subjected to MeCP2 siRNA. G_2 cells were identified with CENPF. (F) ICF fibroblast cells show normal DSB repair. Depletion of DNMT3B partly alleviates the DSB repair defect in the presence of ATMi in ICF G_1 cells. In panels A and C to F, DSB repair was measured by γH2AX focus analysis after 3 Gy of IR. Aphidicolin (4 μM) was added immediately after IR to prevent S-phase cells progressing into G_2 phase and to identify S-phase cells because of extensive γH2AX signaling (A and C to F). Error bars represent the SD from three independent experiments (A to F).

findings suggest MeCP2 contributes to the barrier that HC poses to DSB repair but that the hypomorphic mutations in MeCP2 patient cells do not sufficiently change the HC superstructure to overcome this barrier. An ICF syndrome fibroblast cell line also showed normal DSB repair (Fig. 5F). The addition of ATMi also resulted in the DSB repair defect observed in control cells. DNMT3B depletion partly relieved the repair defect conferred by ATMi addition in control and ICF syndrome cells, although the magnitude was smaller than that observed following MeCP2 depletion.

Cell lines from Rett and ICF syndrome patients exhibit hyperactive IR-induced ATM signaling. Since human fibroblasts do not display the well-defined chromocenters present in MEFs, we could not readily examine γH2AX signal expansion at the HC-DSBs in patient cells. We instead examined downstream events that might be influenced by enhanced γH2AX focus expansion and examined the IR-induced activation of two ATM-dependent phosphorylation events, i.e., ATM autophosphorylation (pATM) and pChk2. To avoid difficulties due to cell cycle stage (e.g., S-phase cells have different chromatin superstructure compared to G_0/G_1-phase cells), we examined contact-inhibited primary cells. Although several Rett syndrome cell lines were available to us, only one line (GM11272) met the criterion of having sufficiently good growth and undergoing contact inhibition to permit this analysis (data not shown). First, we confirmed that Rett cell lines have normal levels of damage response protein expression and ATM-dependent phosphorylation without DNA damage (Fig. 6A and B). After exposure to 0.5 and 3 Gy of IR, we observed enhanced levels of pATM and pChk2 in GM11272 (Rett) cells compared to 48BR (WT) fibroblasts (Fig. 6C), despite the similar numbers of γH2AX foci (Fig. 5C). To substantiate these findings in cycling cells (excluding S-phase cells), we quantified pATM levels in G_1- or G_2-phase GM11272 (Rett)

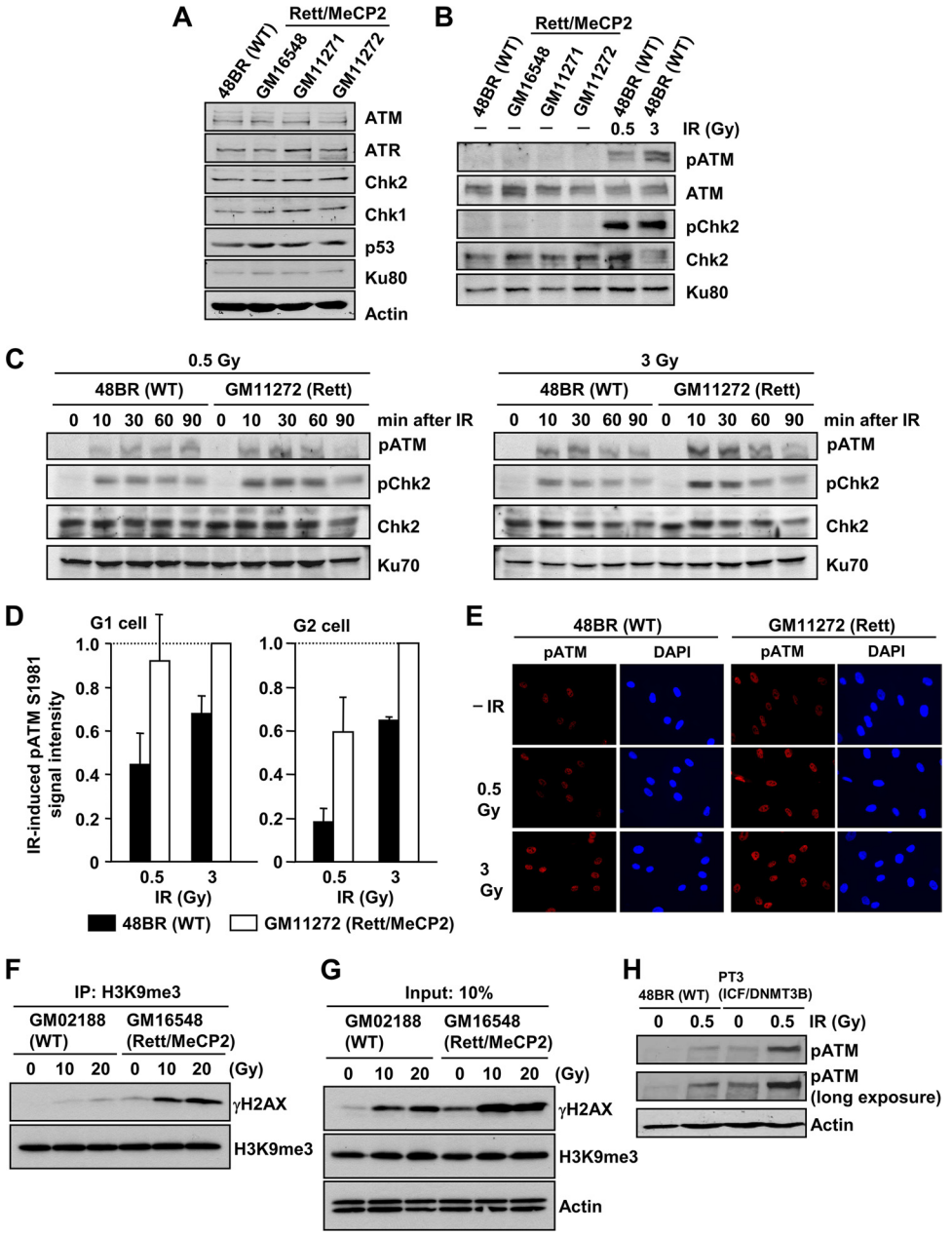

FIG. 6. Rett syndrome cell lines exhibit enhanced ATM signaling after IR. (A) Rett fibroblast cells have normal levels of damage response protein expression. Whole-cell protein extracts were obtained from exponentially growing 48BR (WT) and GM16548, GM11272, and GM11272 (Rett/MeCP2) primary human fibroblast cells. (B) Rett fibroblast cells show normal pATM level without DNA damage. As a positive control, 48BR (WT) cells were irradiated with 0.5 and 3 Gy, and the signals were examined at 30 min after IR. (C) Rett fibroblast G_0/G_1 cells exhibit increased pATM/pChk2 compared to control fibroblasts. Primary 48BR and Rett cells were synchronized in G_0/G_1 with contact inhibition for >10 days. G_0/G_1 arrest was confirmed by fluorescence-activated cell sorting (FACS) (data not shown). (D) Enhanced IR-induced pATM in G_1- and G_2-phase cycling Rett fibroblast cells compared to control fibroblasts. Cycling 48BR and Rett fibroblast cells were irradiated with the indicated doses. Cells were fixed and stained with pATM, CENPF, and DAPI, 30 min after IR. The signal intensity was analyzed using ImageJ. G_2-phase cells were identified by CENP-F. S-phase cells, which show intermediate CENPF levels, were excluded from analysis. Anti-pATM antibody specificity was confirmed as described previously (24). The results represent the means ± the SD from three experiments. (E) The typical images of pATM signal in cycling 48BR and Rett fibroblast cells are shown (40×). (F) Enhanced γH2AX signal in an HC enriched fraction in Rett cells compared to control cells after IR. Lymphoblastoid cell lines (LBLs) were harvested at 30 min after 10 or 20 Gy of IR. To enrich for HC-DNA, the nucleosome fraction was subjected to IP using anti-TriMe K9 histone H3 antibody. (G) Rett LBLs show enhanced global γH2AX signaling after IR. Further, levels of total trimethylated K9 of histone H3 were similar between Rett and control LBLs. (H) ICF fibroblast cells exhibit greater pATM after IR compared to control cells. PT3 (ICF/DNMT3B) cells were arrested in G_0/G_1 following contact inhibition. More than 90% of the cells were in G_1 phase (data not shown). The cells were irradiated with 0.5 Gy, harvested at 1 h after IR, and processed as described above.

cells and in MeCP2 siRNA-treated cells by using IF and cell cycle markers. Consistent with the results obtained following immunoblotting, GM11272 (Rett) cells showed a >2-fold increase in pATM in both G_1 and G_2 phases compared to 48BR (WT) cells (Fig. 6D and E). We also observed a similar increase in MeCP2 siRNA-treated cells (data not shown). We further consolidated the notion that ATM signal expansion is enhanced at the HC-DSBs in Rett syndrome cells by using a co-IP procedure. After IP with α-TriMe K9 histone H3 antibody to immunoprecipitate HC-DNA regions and immunoblotting with γH2AX antibody, we observed that the γH2AX signal in the HC-enriched fraction was substantially greater in Rett syndrome cells compared to control cells (Fig. 6F). Direct immunoblotting with γH2AX antibody showed that the signal was only 2-fold enhanced in Rett syndrome cells compared to control cells (Fig. 6G). These findings are consistent with our IF analysis in NIH 3T3 cells (Fig. 4) and demonstrate that the loss of MeCP2 specifically enhances the encroachment of ATM signaling into HC regions.

In addition, we examined *DNMT3B*-mutated ICF syndrome cells for their ability to activate ATM signaling after IR (Fig. 6H). Although ICF cells have a higher endogenous level of pATM consistent with a previous finding (14), we observed substantially greater pATM levels after IR in ICF syndrome cells compared to control cells. Taken together with the findings presented above, our results suggest that the disordered chromatin present in Rett and ICF syndromes leads to enhanced ATM activation after IR.

Rett syndrome and other disorders with disorganized chromatin show hypersensitive and prolonged G_2/M checkpoint arrest. To investigate whether increased ATM activation has a functional impact, we examined the efficacy of the G_2/M checkpoint arrest after IR. Consistent with previous findings, we observed that WT fibroblasts do not fully activate G_2/M checkpoint arrest after low doses (Fig. 7A). In striking contrast, three different Rett syndrome primary fibroblast lines showed hypersensitive arrest 1 h after IR (Fig. 7A). Full checkpoint arrest was observed in both WT and Rett cells after a dose of 3 Gy since a signal sufficient to activate checkpoint arrest is likely achieved. The addition of a Chk1/Chk2 inhibitor abolished the G_2/M checkpoint arrest in control and Rett cells (Fig. 7B), demonstrating that hypersensitive checkpoint arrest in Rett cells is dependent on ATM-Chk1/Chk2 signaling. Similar analysis of an hTERT immortalized ICF syndrome cell line also revealed hypersensitive checkpoint arrest, which was also abolished by the addition of a Chk1/Chk2 inhibitor (Fig. 7C). Further, MeCP2 and DNMT3B siRNA in 1BR (WT) hTERT cells gave a similar result and MeCP2 siRNA in Rett cells did not show any additivity (Fig. 7D and data not shown). Similar results were also obtained using an LBL derived from HGPS, another disorder impacting on the HC superstructure (Fig. 7E). The control LBL showed more sensitive arrest compared to the fibroblast cell lines, but nonetheless enhanced sensitivity was observed in the HGPS LBL.

Finally, we also examined the maintenance of G_2/M checkpoint arrest. We reasoned that, based on our previous analysis, checkpoint arrest is released when DDR signaling decreases as DSB repair ensues (10). Thus, we predicted that hyperactive checkpoint signaling might manifest as prolonged checkpoint arrest despite a normal rate of DSB repair. Strikingly, cell lines from the patients with impaired HC displayed prolonged G_2/M checkpoint arrest up to 8 h after 2 Gy of IR (a dose which fully activates checkpoint arrest in all cells), whereas control cells are released by 6 h (Fig. 7F). The addition of a Chk1/Chk2 inhibitor at 30 min post-IR, when cells have initiated checkpoint arrest (30), resulted in an immediate release from checkpoint arrest in all cell lines, demonstrating that the prolonged arrest observed in HC disordered patient cells represents hyperactivation of an ATM-Chk1/Chk2-dependent pathway (Fig. 7F). Taken together, our findings demonstrate that the loss of methylation-dependent HC compaction in the Rett and ICF syndromes leads to increased signal expansion at the HC-DSBs, enhanced ATM activation, and hypersensitive G_2/M arrest and maintenance.

MeCP2 expression restores normal G_2/M checkpoint signaling and arrest in MeCP2-depleted cells. To consolidate that the hypersensitive G_2/M checkpoint response in MeCP2-depleted cells is due to the loss of MeCP2 activity, we examined whether the effect could be complemented by the expression of siRNA-resistant MeCP2 cDNA. Although MeCP2 expression in control cells did not affect G_2/M checkpoint sensitivity, MeCP2 expression in MeCP2-depleted cells restores normal G_2/M checkpoint sensitivity (Fig. 8A). A similar, though less marked, impact was also observed when MeCP2 cDNA was expressed in Rett syndrome LBLs (Fig. 8B). The less significant complementation could be due to the reduced transfection efficiency in LBLs compared to hTERT cells, or it could be the consequence of a dominant-negative impact of the mutant protein. Further, MeCP2 expression restored the requirement for ATM for DSB repair to MeCP2 siRNA-treated cells (Fig. 8C).

DISCUSSION

Previous studies have shown that histone H1 restricts DNA damage response (DDR) signaling and that reduced H1 levels confer hypersensitive G_2/M checkpoint arrest (23). We focus here on the impact of the HC superstructure on the DDR since the magnitude of the HC can substantially differ between cell types and because patients with disordered HC have been described (3, 5, 9). Previous studies have demonstrated that HC restricts γH2AX expansion and DSB repair (8, 15, 18). ATM signaling overcomes the barrier posed by HC to DSB repair (15). However, the downstream consequences that HC poses to γH2AX expansion have not been previously examined. Given that only 15 to 20% of DNA is heterochromatic and that, although γH2AX foci only expand on the periphery of HC regions, they rapidly become similar in size to γH2AX foci at the EC regions, it might have been anticipated that any impact would be modest. In fact, the impact of the HC on DDR signaling is marked and only partly relieved by ATM signaling.

In control cells (with functional ATM), we observe faster formation of γH2AX foci at the EC versus HC-DSBs, a finding consistent with previous findings that γH2AX foci rarely form within the core HC region but rather expand on the periphery (8, 15, 18). These previous studies have shown limited overlap between γH2AX foci and HC, which is consistent with the notion that ATM confers localized HC relaxation in the DSB vicinity sufficient to enable HC-DSB repair. Interestingly, by 30

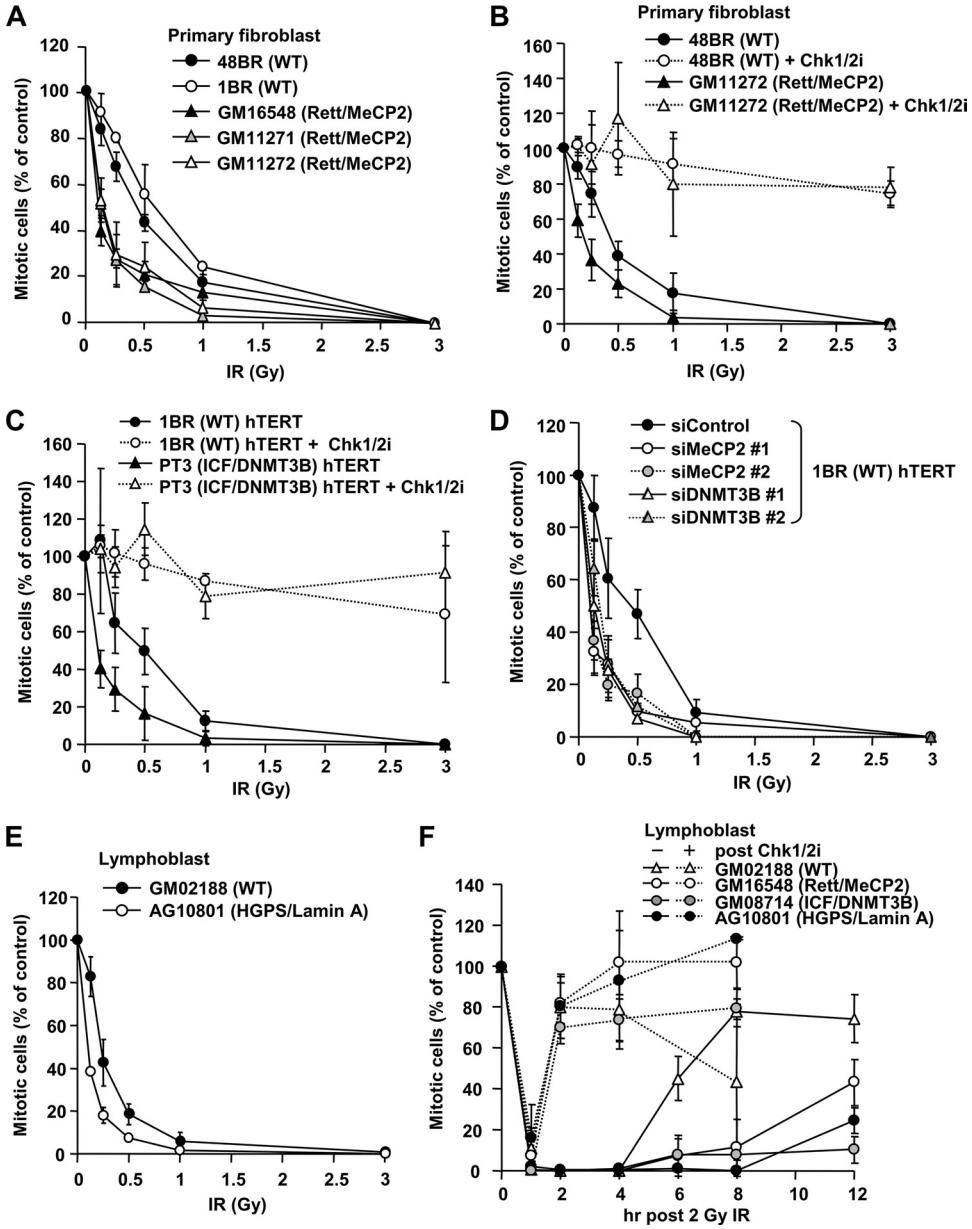

FIG. 7. Cell lines from Rett, ICF, and HGPS patients show hypersensitive IR-induced G_2/M checkpoint arrest. (A) Rett fibroblast cells exhibit hypersensitive G_2/M checkpoint arrest after IR. Two control (48BR and 1BR) and three Rett syndrome (GM16548, GM11271, and GM11272) primary fibroblast lines were analyzed for G_2/M checkpoint arrest. (B) Enhanced initiation of checkpoint sensitivity in Rett fibroblast cells is abolished by adding the Chk1/Chk2 inhibitor. The Chk1/Chk2 inhibitor, SB218078, was added 30 min prior to IR. (C) ICF fibroblast cells show hypersensitive G_2/M checkpoint arrest. 1BR (WT) and PT3 (ICF/DNMT3) hTERT cells were analyzed for G_2/M checkpoint arrest. The inhibitor was added 30 min prior to IR. (D) Depletion of MeCP2 and DNMT3B confers hypersensitive G_2/M checkpoint arrest. 1BR (WT) hTERT cells were subjected to MeCP2 and DNMT3B siRNA. Two distinct siRNA oligonucleotides, 1 and 2, were used for each MeCP2 and DNMT3B knockdown. (E) HGPS patient (AG10801) LBLs show hypersensitive G_2/M checkpoint arrest. (F) LBLs from patients with HC disorder exhibit prolonged G_2/M checkpoint arrest after IR. The maintenance of G_2/M checkpoint arrest was examined in control (GM02188), Rett (GM16548), ICF (GM08714), and HGPS (AG10801) LBLs. LBLs were used for this analysis to allow direct comparison between all patient lines, because efficiently growing HGPS cells were only available as LBLs. Consistent with fibroblast cell lines, Rett and ICF patient LBLs showed hypersensitive initial G_2/M checkpoint arrest after low-dose IR (data not shown). Aphidicolin (APH) at 4 μM was added immediately after 2 Gy of IR. We have not examined 12-h time point in the inhibitor-treated cells because of cellular toxicity by the drug. The mitotic index was measured using p-H3 Ser10 at 1 h after irradiation (A to E). Error bars represent the SD from three independent experiments (A to F).

min post-IR, the sizes of foci at the EC and HC regions are similar.

Depletion of KAP-1, MeCP2, or DNMT3B enhanced the speed and size but not the number of γH2AX foci. For analysis, we divided the DAPI signal intensity into low and high categories, broadly distinguishing EC- and HC-DSBs, respectively. However, it has to be appreciated that there is a range of heterochromatinization and that this represents a somewhat

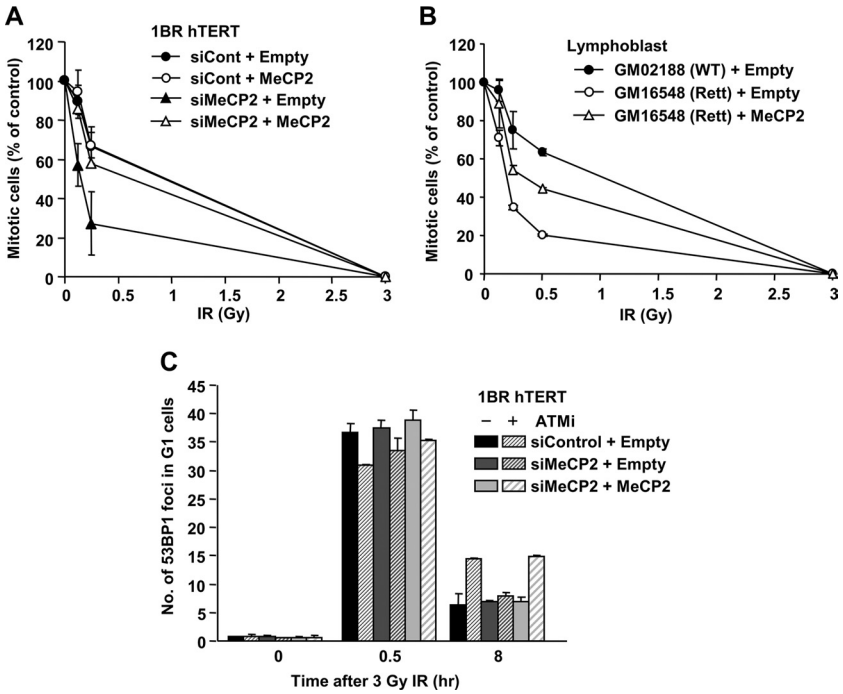

FIG. 8. MeCP2 expression restores normal G_2/M checkpoint signaling and arrest in MeCP2-defective cells. (A) MeCP2 expression in MeCP2-depleted cells restores normal G_2/M checkpoint arrest. siRNA-resistant WT MeCP2 was expressed in 1BR (WT) hTERT cells with or without depletion of endogenous MeCP2 proteins. (B) MeCP2 expression in Rett LBL cells partially rescues the hypersensitive G_2/M checkpoint arrest. (C) MeCP2 expression in MeCP2-depleted cells restores the requirement for ATM for DSB repair to MeCP2 siRNA-treated cells. DSB repair in G_1 cells was measured by 53BP1 focus analysis after 3 Gy of IR. The mitotic index was measured using p-H3 Ser10 at 1 h after irradiation (A and B). Error bas represent the SD from two or three independent experiments (A to C).

crude division. KAP-1 siRNA impacted primarily at DSBs with the highest DAPI density, which is consistent with KAP-1 being predominantly localized at highly compacted HC; the impact for MeCP2 was broader, possibly reflecting the presence of methylated CpGs in a wider range of compacted regions (although predominantly in HC-DNA). Surprisingly, under these conditions γH2AX focus sizes at the HC-DSBs became even larger than at the EC-DSBs. One possibility is that dynamic but distinct chromatin changes occur at the EC versus the HC regions. At the HC-DSBs, it is necessary to achieve relaxation since HC is a barrier to repair, while there may be processes that actually restrict γH2AX focus expansion at the EC-DSBs. For example, several recent studies have reported that CHD4, a global chromatin remodeling component associated with HDAC activity, is recruited to DSBs after IR (20, 27, 32). In addition, recent studies have suggested that transcription is silenced at transcriptionally active DSBs and/or restricts γH2AX focus expansion (17, 29). These dynamic changes may tend to diminish signaling at EC-DSBs but enhance it at HC-DSBs. Our analysis of cells lacking 53BP1, which promotes concentrated pKAP-1 at HC-DSBs but does not affect pan-nuclear pKAP-1 (24), shows specific restriction in the expansion of HC-DSBs strongly suggesting that one function of ATM is to enhance signaling from HC-DSBs (ATM may, however, also perturb expansion at EC-DSBs). Thus, the result of perturbed HC superstructure when ATM signaling is active may be elevated signal expansion at HC-DSBs relative to EC-DSBs. Our analysis of the overlap between γH2AX foci and regions of high DAPI density by two- and three-dimensional modeling was particularly informative. These findings show that knockdown of HC components (KAP-1, MeCP2, and DNMT3B) enhances γH2AX focus expansion into the HC core to a greater extent than that observed in control cells, which is consistent with the notion that ATM signaling only relaxes HC in the DSB vicinity and that most γH2AX focus expansion occurs into the neighboring EC region (15). Thus, ATM only minimally and locally overcomes the barrier posed by HC to γH2AX focus expansion. Hence, γH2AX expansion following the depletion of core HC factors is greater and progresses further into the HC core than in control cells.

γH2AX acts as a scaffold to recruit MDC1, MRN, and 53BP1, which together aid ATM retention at the DSB (25). Thus, it might be anticipated that focus size correlates with the magnitude of the downstream response. However, cells lacking γH2AX show efficient DDR signaling and checkpoint arrest except at low IR doses (12). We therefore examined checkpoint signaling at early times after low doses and observed enhanced ATM signaling following KAP-1 or MeCP2 depletion to be most evident from 10 to 60 min post-IR. Previously, we reported that the G_2/M checkpoint is insensitive and is not activated by low IR doses (10). Strikingly, we observed that depletion of KAP-1, MeCP2, or DNMT3B by siRNA permits hyperactivation of checkpoint arrest at low doses that fail to arrest control cells. Thus, the impact of HC provides one explanation for the lack of sensitivity of the G_2/M checkpoint. Our findings described above are consistent with a recent report that HC can be induced by oncogenic stress and that such HC formation can restrict activation of the DNA damage re-

sponse and, most importantly, signaling to apoptosis (11). This important finding consolidates our results and shows that HC arising in a distinct manner can exert a similar dampening impact on the damage response.

A major focus of our work is the examination of disorders with aberrant HC. We focused on Rett syndrome partly because we observed the most dramatic impact in these cells and because they grew well, had low endogenous γH2AX focus numbers and DDR signaling. Rett syndrome cells show an ~2-fold increase in ATM phosphorylation, hypersensitive checkpoint activation, and prolonged checkpoint maintenance, all features consolidated using siRNA-mediated depletion of MeCP2. We did not examine downstream steps of ATM signaling (e.g., Chk2 phosphorylation) in ICF or HGPS cells due to difficulties in obtaining sufficient G_0/G_1 cells. However, the checkpoint analysis verified hypersensitive arrest and prolonged G_2/M checkpoint activation, which is consistent with enhanced IR-induced ATM activation. A previous study reported elevated endogenous pATM in ICF LCLs without obvious changes in the response to IR (14). However, different methodologies were used, and the subtle response to low doses was not examined. Collectively, these findings provide a clinical relevance to our work and show that disorders with impaired HC structure can display enhanced DDR signaling.

A range of studies have shown that the sensitivity and duration of checkpoint arrest reflects the status of DSB repair. Changes to chromatin structure, including epigenetic histone modifications have been shown to influence checkpoint arrest via an impact on DSB repair (22, 27). Here, we observed normal DSB repair. Thus, our findings provide a novel example of prolonged checkpoint arrest despite normal DSB repair and demonstrate that the checkpoint response can be markedly affected by the level and degree of HC compaction. We identify syndromes with disordered HC as displaying an abnormal checkpoint response despite normal DSB repair.

A significant question is whether enhanced DDR signaling impacts clinically. We did not observe any significant change in IR sensitivity in primary Rett syndrome fibroblasts (data not shown). However, in primary fibroblasts survival is likely determined predominantly by DSB repair, which was normal in Rett syndrome cells. Prolonged arrest may simply lead to delayed cell cycling without a significant impact on survival. However, the response may depend upon cell type; for example, in cells that activate apoptosis (which does not occur following IR in primary fibroblasts), elevated signaling may enhance cell death. Further, enhanced signaling from uncapped telomeres could manifest as early-onset senescence following telomere erosion. Significantly, premature aging is a phenotype of syndromes with disordered chromatin. Finally, the magnitude of HC compaction may differ between stem and differentiated cells, potentially influencing the magnitude of ATM signaling. More specific studies are required to address these questions.

In summary, we have shown an unexpectedly large impact on DDR signaling following the loss of proteins that impact upon HC superstructure. The results reveal that the HC superstructure is a barrier to DDR signaling that is partly, but not totally, relieved by ATM signaling. We show that HC relaxation conferred by patient mutations or by knockdown of HC proteins has downstream consequences, including hyperactive ATM signaling and checkpoint arrest, which cannot be attributed to impaired DSB repair. Thus, the barrier that HC superstructure poses to checkpoint signaling provides one explanation for the insensitivity of G_2/M checkpoint arrest.

ACKNOWLEDGMENTS

The P.A.J. laboratory is supported by the Medical Research Council, the Association for International Cancer Research, the Department of Health, and the Wellcome Research Trust.

REFERENCES

1. **Adams, J. M., and S. Cory.** 1998. The Bcl-2 protein family: arbiters of cell survival. Science **281:**1322–1326.
2. **Agarwal, N., et al.** 2007. MeCP2 interacts with HP1 and modulates its heterochromatin association during myogenic differentiation. Nucleic Acids Res. **35:**5402–5408.
3. **Amir, R. E., et al.** 1999. Rett syndrome is caused by mutations in X-linked MECP2, encoding methyl-CpG-binding protein 2. Nat. Genet. **23:**185–188.
4. **Anstey, A. V., et al.** 1999. Characterization of photosensitivity in the Smith-Lemli-Opitz syndrome: a new congenital photosensitivity syndrome. Br. J. Dermatol. **141:**406–414.
5. **Barber, J. B., et al.** 2000. Relationship between in vitro chromosomal radiosensitivity of peripheral blood lymphocytes and the expression of normal tissue damage following radiotherapy for breast cancer. Radiother. Oncol. **55:**179–186.
6. **Beucher, A., et al.** 2009. ATM and Artemis promote homologous recombination of radiation-induced DNA double-strand breaks in G_2. EMBO J. **28:**3413–3427.
7. **Chiolo, I., et al.** 2011. Double-strand breaks in heterochromatin move outside of a dynamic HP1a domain to complete recombinational repair. Cell **144:**732–744.
8. **Cowell, I. G., et al.** 2007. γH2AX foci form preferentially in euchromatin after ionizing-radiation. PLoS One **2:**e1057.
9. **Dechat, T., et al.** 2008. Nuclear lamins: major factors in the structural organization and function of the nucleus and chromatin. Genes Dev. **22:**832–853.
10. **Deckbar, D., et al.** 2007. Chromosome breakage after G_2 checkpoint release. J. Cell Biol. **176:**748–755.
11. **Di Micco, R., et al.** 2011. Interplay between oncogene-induced DNA damage response and heterochromatin in senescence and cancer. Nat. Cell Biol. **13:**292–302.
12. **Fernandez-Capetillo, O., et al.** 2002. DNA damage-induced G_2-M checkpoint activation by histone H2AX and 53BP1. Nat. Cell Biol. **4:**993–997.
13. **Fernet, M., F. Megnin-Chanet, J. Hall, and V. Favaudon.** 2010. Control of the G_2/M checkpoints after exposure to low doses of ionizing radiation: implications for hyper-radiosensitivity. DNA Repair (Amsterdam) **9:**48–57.
14. **Goldstine, J. V., et al.** 2006. Constitutive phosphorylation of ATM in lymphoblastoid cell lines from patients with ICF syndrome without downstream kinase activity. DNA Repair (Amsterdam) **5:**432–443.
15. **Goodarzi, A. A., et al.** 2008. ATM signaling facilitates repair of DNA double-strand breaks associated with heterochromatin. Mol. Cell **31:**167–177.
16. **Guenatri, M., D. Bailly, C. Maison, and G. Almouzni.** 2004. Mouse centric and pericentric satellite repeats form distinct functional heterochromatin. J. Cell Biol. **166:**493–505.
17. **Iacovoni, J. S., et al.** 2010. High-resolution profiling of gammaH2AX around DNA double strand breaks in the mammalian genome. EMBO J. **29:**1446–1457.
18. **Kim, J. A., M. Kruhlak, F. Dotiwala, A. Nussenzweig, and J. E. Haber.** 2007. Heterochromatin is refractory to gamma-H2AX modification in yeast and mammals. J. Cell Biol. **178:**209–218.
19. **Kurz, E. U., and S. P. Lees-Miller.** 2004. DNA damage-induced activation of ATM and ATM-dependent signaling pathways. DNA Repair (Amsterdam) **3:**889–900.
20. **Larsen, D. H., et al.** 2010. The chromatin-remodeling factor CHD4 coordinates signaling and repair after DNA damage. J. Cell Biol. **190:**731–740.
21. **Lobrich, M., et al.** 2010. γH2AX foci analysis for monitoring DNA double-strand break repair: strengths, limitations, and optimization. Cell Cycle. **9:**662–669.
22. **Miller, K. M., et al.** 2010. Human HDAC1 and HDAC2 function in the DNA-damage response to promote DNA nonhomologous end-joining. Nat. Struct. Mol. Biol. **17:**1144–1151.
23. **Murga, M., et al.** 2007. Global chromatin compaction limits the strength of the DNA damage response. J. Cell Biol. **178:**1101–1108.
24. **Noon, A. T., et al.** 2010. 53BP1-dependent robust localized KAP-1 phosphorylation is essential for heterochromatic DNA double-strand break repair. Nat. Cell Biol. **12:**177–184.
25. **Panier, S., and D. Durocher.** 2009. Regulatory ubiquitylation in response to DNA double-strand breaks. DNA Repair (Amsterdam) **8:**436–443.
26. **Paull, T. T., et al.** 2000. A critical role for histone H2AX in recruitment of repair factors to nuclear foci after DNA damage. Curr. Biol. **10:**886–895.
27. **Polo, S. E., A. Kaidi, L. Baskcomb, Y. Galanty, and S. P. Jackson.** 2010.

Regulation of DNA-damage responses and cell-cycle progression by the chromatin remodeling factor CHD4. EMBO J. **29:**3130–3139.
28. **Riballo, E., et al.** 2004. A pathway of double-strand break rejoining dependent upon ATM, Artemis, and proteins locating to gamma-H2AX foci. Mol. Cell **16:**715–724.
29. **Shanbhag, N. M., I. U. Rafalska-Metcalf, C. Balane-Bolivar, S. M. Janicki, and R. A. Greenberg.** 2010. ATM-dependent chromatin changes silence transcription in cis to DNA double-strand breaks. Cell **141:**970–981.
30. **Shibata, A., et al.** 2010. Role of ATM and the damage response mediator proteins 53BP1 and MDC1 in the maintenance of G_2/M checkpoint arrest. Mol. Cell. Biol. **30:**3371–3383.
31. **Shumaker, D. K., et al.** 2006. Mutant nuclear lamin A leads to progressive alterations of epigenetic control in premature aging. Proc. Natl. Acad. Sci. U. S. A. **103:**8703–8708.
32. **Smeenk, G., et al.** 2010. The NuRD chromatin-remodeling complex regulates signaling and repair of DNA damage. J. Cell Biol. **190:**741–749.
33. Reference deleted.
34. **Uziel, T., et al.** 2003. Requirement of the MRN complex for ATM activation by DNA damage. EMBO J. **22:**5612–5621.
35. **Wade, P. A.** 2001. Methyl CpG binding proteins: coupling chromatin architecture to gene regulation. Oncogene **20:**3166–3173.